High Strain Piezoelectric Multilayer Actuators—A Material Science and Engineering Challenge

C.A. RANDALL,[1] A. KELNBERGER,[1,2] G.Y. YANG,[1] R.E. EITEL[1*] & T.R. SHROUT[1]

[1]*Center for Dielectric Studies, The Pennsylvania State University, University Park, PA 16802, USA*
[2]*Robert Bosch GmbH, Dept. FV/FLW, Postfach 10 50 60, D-700 Stuttgart, Germany*

Abstract. Piezoelectric actuators are at an important stage of their development into a large component market. This market pull is for dynamically driven actuators for Diesel injector valves in automobiles. Cost, yield, and reliability are important concerns for the automobile industry. A number of these concerns relate back to basic material science issues in the manufacture of the piezoelectric actuators. This paper discusses material development of the piezoelectric ceramic and new opportunities for higher temperature materials. An important consideration in developing low-fire ceramics is the flux selection for a given system, and these must be selected to limit electrode-ceramic interface reactions in both Ag/Pd and copper-metallized electrode actuators.

Keywords: piezoelectrics, electrode interface, multilayers, actuators, copper, Ag-Pd

Introduction

Cofired multilayer piezoelectric actuators have long been demonstrated for a wide variety of electromechanical applications requiring precision positioning over short time scales. In smart systems, sensors and multilayer actuators are combined with feedback control circuitry, to adapt and modify structures to the environment. Despite research and practical demonstrations in such systems, piezoelectric actuator markets have been niche with the result that piezoelectric actuators have only been manufactured in small quantities, in contrast to multilayer ceramic capacitors and varistors. The recent introduction of piezoelectric actuators in fuel injector systems for state-of-the-art diesel automobiles will soon change all this, due to the large-scale availability of cheap piezoelectric actuators. In preparation for this new revolution, which could result in the production of over 10^8 actuators per year, we review some of the key material science issues that need to be considered to improve piezoelectric multilayer actuator performance, yield, reliability and cost. In this paper, we specifically focus on electrode-piezoelectric ceramic selection, interfacial interactions, flux compatibility, and reliability issues.

## Piezoelectric Actuators for Diesel Fuel Injection

Piezoelectric actuators are being considered to replace electromagnetic solenoid valves in diesel injection in a so-called "Common Rail" system, Fig. 1(a) (Photo Bosch) [1]. Through careful design of the injector, the piezoelectric actuator can offer a number of attractive advantages over traditional solenoids, including easy starting, increased fuel efficiency, low CO_2 emissions, and low engine noise [2]. These advantages are reaped owing to the high-speed operation and the flexibility of the control of injector processes. The response of the nozzle needle is less than 0.0001 seconds. This fast response speed reduces the fuel delivery rate and in turn the energy required from the high-pressure fuel pump. Furthermore, more sophisticated injection processes can be designed to also increase efficiency of the combustion process. A typical injector system is schematically represented in Fig. 1(b) with the position of the multilayer actuator indicated [3]. The general

*To whom all correspondence should be addressed.
E-mail: car4@psu.edu

Common Rail System for 8-Cylinder Passenger Car Diesel Engines
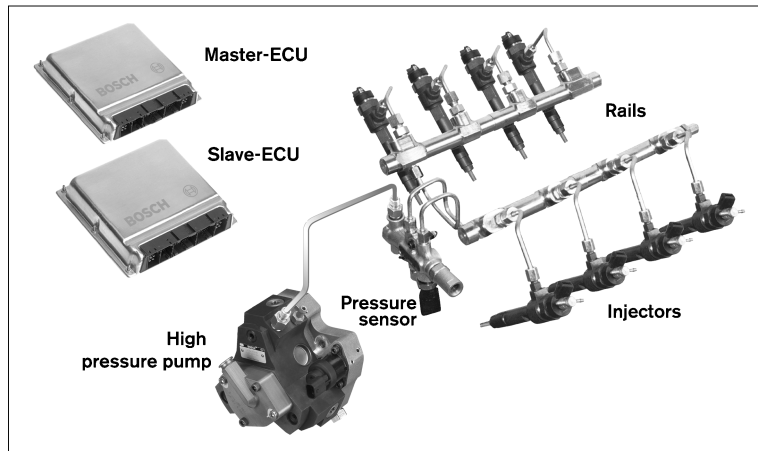
(a)
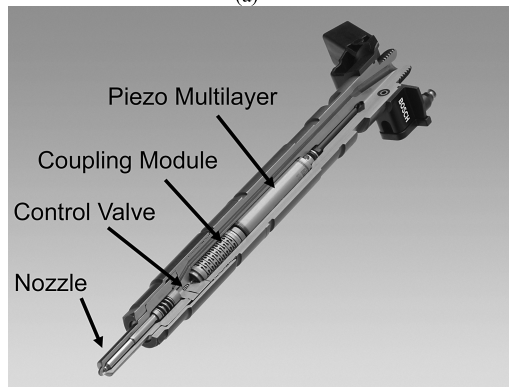
(b)

Fig. 1. (a) Common rail injection system for an 8-cylinder Diesel engine, and (b) schematic of piezoelectric injector. (Photos: BOSCH)

requirements are control of the stroke amplitude, the speed of the stroke and the blocking pressure the actuator can supply. These basic requirements need a high piezoelectric coefficient material that is designed into a device that can quickly be charged and is elastically stiff. The precise designs of both the injector and the actuators vary from system to system. Specifically, the geometry, electromechanical performance, capacitance, and drive circuitry of the actuator all vary. So unlike the production of multilayer capacitor and varistor devices there is no standardization and hence actuator components are constructed on a customer specific basis.

The major effort in the scaling up multilayer piezoelectric actuators for diesel fuel injection is in Europe, where approximately 40% of automobiles are diesel.

However, in the long term, these injection systems will expand to gasoline-based vehicles, thereby revolutionizing the whole automobile industry and drastically expanding the piezoelectric ceramic industry [3]. Furthermore, with the availability of low cost actuators, many of the "smart" systems that have been previously discussed become more likely and cost-effective.

Piezoelectric Materials

Piezoelectric effects are observed in a large number of materials; with the general requirement of noncentrosymmetry in the crystal structure. At this time, the most important commercial piezoelectric material

is quartz, SiO_2, which is used in timing devices and surface acoustic wave filters in single crystal form. Quartz does not have a large piezoelectric coefficient, but it has the ability to have extremely low electromechanical losses, and in certain crystallographic cuts has essentially temperature independent electromechanical properties [4]. To obtain non-centrosymmetry behavior in polycrystalline materials, the macroscopic symmetry of the system has to be broken in some way. If the material is ferroelectric, a subset of the piezoelectric family, the material undergoes a phase transition to produce a spontaneous polarization below a critical phase transition temperature (T_c). Then under the application of a sufficiently strong field, the spontaneous polarization can be aligned into a metastable state, the so-called poling process. This state has macroscopical non-centrosymmetry and is therefore piezoelectric. All poled ferroelectric materials are piezoelectric, but again, there is a large variation in the important piezoelectric coefficients across different materials [5].

The key piezoelectric coefficients that are typically considered are the direct and converse piezoelectric effect. The direct piezoelectric effect involves the application of force of stress to a piezoelectric material to produce a charge density change on the surface of the material, namely

$$P_i = d_{ijk} X_{jk}$$

where polarization is directly proportional to the applied stress, P_i is a vector component, X_{jk} is the stress tensor, and d_{ijk} is the third rank tensor of the direct piezoelectric effect. It is a necessary condition of non-centrosymmetry that gives non-zero d_{ijk} coefficients; the number and direction of non-zero coefficients are dependent upon symmetry in a single crystal, and similarly, defined relative to the poling direction in a polycrystalline ferroelectric ceramic [6].

The converse piezoelectric effect involves the application of an electric field to a piezoelectric material to produce a strain in the material according to

$$x_{jk} = d_{ijk} E_i$$

where x_{jk}—strain tensor, d_{ijk} is the converse piezoelectric equivalent in magnitude and direction to the direct piezoelectric coefficient tensor, and E_i is the electric field vector. It is the converse piezoelectric effect that is utilized in piezoelectric actuators. The magnitude of the d_{ijk} coefficient that is of particular importance in material selection and design of a multilayer actuator and can be regarded as a simple figure of merit. The coefficients are typically reported in the matrix notation for piezoelectric ceramic applications, so we are concerned with d_{33}, d_{31}, and sometimes d_{15}. The poling direction is by convention in the 3-direction, and therefore 33 indicates the electric field is applied parallel to the poling direction, producing a strain in the same direction. The multilayer actuator is mostly concerned with d_{33} in the converse piezoelectric effect; specifically, fuel injector actuator requires high field strain corresponding to $d_{33} \sim 550$ pC/m^2 over a temperature range –55 to 150°C.

Piezoelectric Ceramics

Piezoelectric ceramics have been researched for a wide variety of actuator, sensor, and motor applications for the past 25 years. For most applications, the compositions have been based on the binary system $(1-x)$PbZrO$_3$–(x)PbTiO$_3$,(PZT) building on the pioneering work of Berlincourt, Jaffe, Cook, and Jaffe and others [6, 7]. These PZT materials are a solid solution with the perovskite structure, which has a twelve-fold coordinated A-site cation, and a small B-site cation in octahedral coordination. There are other crystal structures that are piezoelectric; however, all the important piezoelectric coefficients are typically inadequate for the injection applications.

One key aspect of the piezoelectric perovskite ceramic, $(1-x)$PbZrO$_3$-(x)PbTiO$_3$ (PZT) solid solution is a phase boundary between a tetragonal (F_T) and a rhombohedral (F_R) (HT) ferroelectric symmetries, as shown in Fig. 2(a). This phase boundary is often referred to as a morphotropic phase boundary (MPB). The MPB compositions have mixed symmetries and therefore are easily poled in the polycrystalline form. In addition, the electromechanical properties are enhanced at these phase boundaries. Above the ferroelectric phase transition (T_c) at ~350°C for the $x = 0.48$ MPB composition, PZT is in the prototype or paraelectric phase. The crystallographic symmetry of this prototype perovskite phase is Pm3m, a cubic centrosymmetric space group. Below T_c, a mix of ferroelectric rhombohedral and tetragonal phases exists.

Often a ternary solid solution is also considered as a basic composition for piezoelectric ceramics. This involves the addition of a complex B-site lead perovskite, with general chemical formula Pb(B$_1$B$_2$)O$_3$ [8, 9].
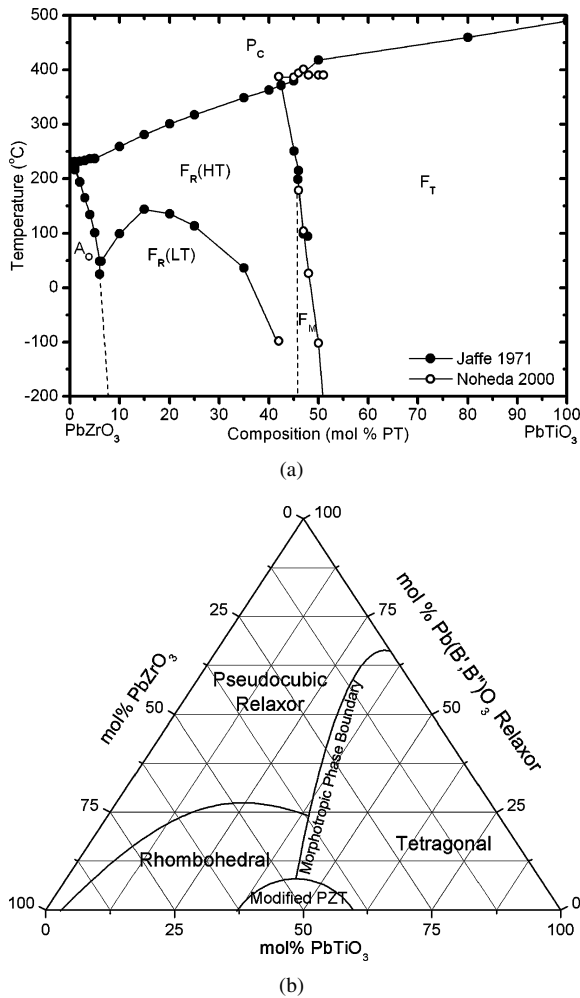
(a)

(b)

Fig. 2. Binary phase diagram indicating ferroelectric and related phase field between $PbZrO_3$–$PbTiO_3$, and (b) ternary phase designs between $Pb(B'B'')O_3$–$PbZrO_3$ and $PbTiO_3$.

Here B_1 and B_2 have to stoichiometrically balance to a +4 valence, and then involve cations such as Zn^{+2}, Mg^{+2}, Co^{+2}, Sc^{+3}, etc., and larger valence cations such as Nb^{+5}, Ta^{+5}, W^{+6}, etc. These complex lead perovskites are frequently relaxor ferroelectric materials, such as $Pb(Ni_{1/3}Nb_{2/3})O_3$, $Pb(Mg_{1/3}Nb_{2/3})O_3$, $Pb(Zn_{1/3}Nb_{2/3})O_3$. These compounds also have a MPB and enhanced piezoelectric properties at the boundary. When all combined in a ternary phase diagram, a MPB exists continuously, from one binary to the other, as illustrated in Fig. 2(b). In the case of solid solutions with $Pb(Ni_{1/3}Nb_{2/3})O_3$, there are added advantages in the enhanced sintering kinetics, which lower the fir-

ing temperature and allow better control over volatile species, such as the PbO. In addition to the piezoelectric coefficient magnitude, the diesel engine actuators require a high T_c, as the piezoelectric has to operate without depoling up to a temperature of $150°C$. Any depoling increases electromechanical losses and changes capacitance of the injectors. In order to limit depoling, ferroelectric transitions of $T_c > 350°C$ are generally required.

Recently, with the discovery of perovskite structured $(1−x)Bi(Me^{+3})O_3$-$xPbTiO_3$ and $(1−x)Bi(Me_1Me_2)O_3−x$ $PbTiO_3$ solid solutions, higher transition MPBs were found with high electromechanical properties [10–15]. In the $(1 − x)BiScO_3$-$xPbTiO_3$ system, for example, a MPB is found at $x = 0.64$ with $T_c \sim 450°C$ and a $d_{33} \sim 450$–500 pC/N, and $(1 − x)Bi(Mg_{1/2}Ti_{1/2})O_3$–$xPbTiO_3$ has an MPB at $x = 0.38$ with $T_c \sim 470°C$ and $d_{33} \sim 240$ pC/N. These new perovskite-based compositions can be considered individually as binary-based formulations for high strain, high T_c piezoelectrics or combined into ternaries with either $PbZrO_3$ or $Pb(B_1B_2)O_3$ end members. It is clear from Table 1 that there is a large compositional space to be considered with $(1 − x)Bi(Me_1Me_2)O_3−xPbTiO_3$ binaries and also new ternaries [16]. Considering these approaches, there may be more compositions to consider in the Bi systems than in the extensively studied Pb-based piezoelectric ceramics.

To enhance and optimize the piezoelectric properties of a high strain material, it is necessary to obtain a unipolar high field d_{33}, as illustrated in Fig. 3, at values ~ 550 pC/N to 700 pC/N for the fuel injector multilayer actuator. To achieve these high levels of
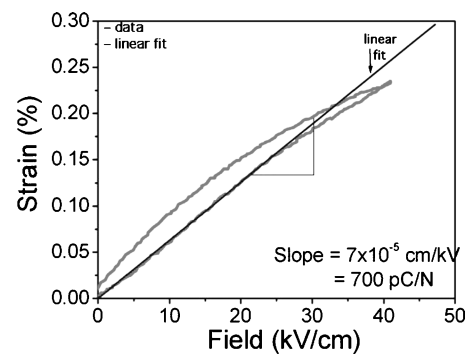

Fig. 3. Unipolar high field strain behavior in soft piezoelectric materials.

Table 1. Bi(Me′Me″)O$_3$-PbTiO$_3$-Perovskite binary systems.

BiMe^{+3}O$_3$-PbTiO$_3$	Bi(Me$^{+2}_{1/2}$Me$^{+4}_{1/2}$)O$_3$-PbTiO$_3$	Bi(Me$^{+2}_{2/3}$Me$^{+5}_{1/3}$)O$_3$-PbTiO$_3$	Bi(Me$^{+2}_{3/4}$Me$^{+6}_{1/4}$)O$_3$-PbTiO$_3$
BiFeO$_3$-PbTiO$_3$	Bi(Mg$_{1/2}$Ti$_{1/2}$)O$_3$-PbTiO$_3$	Bi(Mg$_{2/3}$Nb$_{1/3}$)O$_3$-PbTiO$_3$	Bi(Mg$_{3/4}$W$_{1/4}$)O$_3$-PbTiO$_3$
BiMnO$_3$-PbTiO$_3$	Bi(Zn$_{1/2}$Ti$_{1/2}$)O$_3$-PbTiO$_3$	Bi(Zn$_{2/3}$Nb$_{1/3}$)O$_3$-PbTiO$_3$	Bi(Co$_{3/4}$W$_{1/4}$)O$_3$-PbTiO$_3$
BiCuO$_3$-PbTiO$_3$	Bi(Co$_{1/2}$Ti$_{1/2}$)O$_3$–PbTiO$_3$	Bi(Mg$_{2/3}$Ta$_{1/3}$)O$_3$-PbTiO$_3$	
BiScO$_3$-PbTiO$_3$	Bi(Mg$_{1/2}$Zr$_{1/2}$)O$_3$-PbTiO$_3$	Bi(Zn$_{2/3}$Ta$_{1/3}$)O$_3$-PbTiO$_3$	
BiInO$_3$-PbTiO$_3$	Bi(Zn$_{1/2}$Zr$_{1/2}$)O$_3$-PbTiO$_3$	Bi(Co$_{2/3}$Ta$_{1/3}$)O$_3$-PbTiO$_3$	
BiGaO$_3$-PbTiO$_3$	Bi(Mg$_{1/2}$Sn$_{1/2}$)O$_3$-PbTiO$_3$	Bi(Co$_{2/3}$Nb$_{1/3}$)O$_3$-PbTiO$_3$	
BiYbO$_3$-PbTiO$_3$			

strain it is necessary to donor dope the basic binary and ternary systems discussed above and have a microstructure with grain sizes > ~2 to 4 μm. In the simple case of the PbZrO$_3$–PbTiO$_3$, donors are typically added as La$^{\bullet}_{Pb}$ or Bi$^{\bullet}_{Pb}$ to the A-site, or with Nb$^{\bullet}_{Ti}$, W$^{\bullet\bullet}_{Ti}$, or Sb$^{\bullet}_{Ti}$ to the B-site [17–19]. In some cases, $F^{\bullet}_o$ is added to the anion sublattice as a donor. Here we express the dopants in the classical Kroger-Vink notation. It is important to note that many of the dopants lower the transition temperature, T_c, for example, ~−20°C/per atom% with La^{+3} [20].

Donor substitution is believed to reduce oxygen vacancy concentration and also enhance ferroelectric domain wall mobility, which gives rise to an additional extrinsic piezoelectric response over the lattice single domain contribution often termed the intrinsic response [21–23]. The response of a non-180°C domain wall with an applied electric field effectively gives rise to an extrinsic strain. Acceptor doping such as Fe$^{+3}_{Ti}$ creates additional defect dipoles with associated oxygen vacancies beyond the V$''_{Pb}$ − V$^{\bullet\bullet}_o$ pairs [24]. These defect dipoles limit non-180° domain wall motion and thereby limit the total piezoelectric response to levels insufficient for the high strain actuators required for diesel injection.

The total donor content has to consider that its incorporation can shift the position of the MPB, and the Zr/Ti ratio may have to be adjusted for optimal piezoelectric performance. It should also be noted that lead oxide is highly volatile species and lead loss can lead to the development of ionically compensated [V$''_{Pb}$] = [V$^{\bullet\bullet}_o$] pairs, which can naturally harden the material and lower the d_{33} performance [6]. In addition to intrinsically produced acceptoric defects such as lead vacancies, we have to be concerned with incorporation of foreign acceptors from raw material selection or introduction during the milling process, such as Y$'_{Ti}$ from YSZ (yttrium stabilized zirconia) media.

It is important to note that accompanying increased movement of non-180° domain walls, there is often an enhanced hysteresis. This is the result of irreversible displacement of the domain walls, leading to a non-linear and hysteretic piezoelectric response at relatively low driving fields [24]. In designing such materials, it is important to consider that a piezoelectric coefficient is a complex coefficient

$$d^*_{mn} = d'_{mn} - jd''_{mn}$$

where d'_{mn} is the real component of the piezoelectric coefficient and d''_{mn} is the imaginary coefficient, and $j = \sqrt{-1}$ (note mn are the matrix notation of the tensors). The piezoelectric loss has to be minimized, as it is a source of heating under high drive and high duty cycles in the injection operation. One of the most informative approaches to investigate the relative performance of one piezoelesctric material against another is to consider the Rayleigh law analysis [25–28]. The dielectric equations illustrate the dependence of the permittivity (ε_{33}) and polarization (P_3) as a function of the amplitude of the AC electric field (E_o). Similarly, the field dependence of the piezoelectric coefficient (d_{33}) can be described. Separate Rayleigh parameters (ε_{int} and α) and (d_{int} and α) are determined from the response. A further and necessary consequence of the application of the Rayleigh law is the generation of odd order harmonics in expansions that describe the locus of the hysteresis. The mathematical form of the equations for the polarization or the strain loop is similar and given by:

$$P = P_{\max}\sin(\omega t)\frac{4\alpha E_o^2}{3\pi}\cos\omega t - \frac{4\alpha E_o^2}{\pi}$$
$$\times \left(\frac{1}{15}\cos(3\omega t) + \frac{1}{105}\cos(3\omega t) + L\right)$$
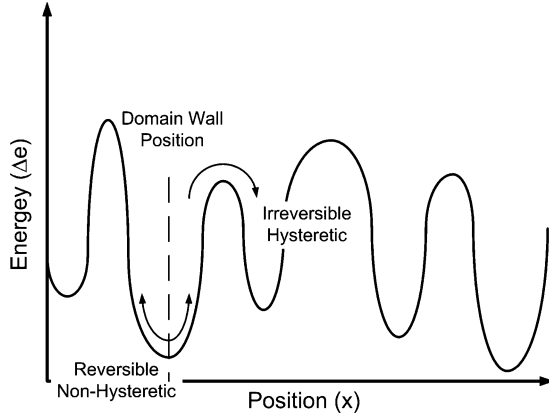$$\omega - \text{angular frequency (s}^{-1}).$$

Fig. 4. Motion of a non-180° domain wall through a random potential created by defect pinning sites.

Analysis of the data using a Fourier transform can be used to determine the various harmonics. Once the basic Rayleigh criteria have been established, the real part of the ε' and d' can be taken from the slopes of the loops, the hysteresis loss energy is the area of the loops and the loss can be extracted from this information. So collectively, we can determine high field information on real and imaginary components of the permittivity $\varepsilon^* = \varepsilon' - j\varepsilon''$, and $d^* = d' - jd''$.

Recently, the Rayleigh law has been successfully used to model non-linear hysteretic response in ferroelectric ceramics and thin films. The strength of the Rayleigh model is in its ability to quantify both the dielectric and piezoelectric response and their respective losses. The Rayleigh model may be applied to the motion of any interface through a random potential, similar to those represented in Fig. 4. In ferroelectrics, the Rayleigh approach describes both the reversible and irreversible domain wall motion through a random distributions of domain pinning sites.

The dielectric response can then be described by:

$$P = \varepsilon_{\text{int}} E_o + \alpha E_o^2 \quad \text{and}$$

$$\varepsilon_{33} = \varepsilon_{\text{int}} + \alpha E_o$$

$$P_3 = (\varepsilon_{\text{init}} + E_o)E \pm \frac{1}{2}\left(E_o^2 - E^2\right)$$

and similarly, the converse piezoelectric response has the same form:

$$x_3 = d_{\text{int}} E_o + \alpha E_o^2$$

$$d_{33} = d_{\text{int}} + \alpha E_o$$

$$x_3 = (d_{\text{int}} + \alpha E_o)E \pm \frac{\alpha}{2}\left(E_o^2 - E^2\right)$$

The Rayleigh analysis is mostly being considered to understand material polarization mechanisms, but it is believed that this methodology is also of practical interest for multilayer actuators design and control optimization enabling a full response characterization over a broad base of operating conditions with temperature, frequency, and field. With such analysis the device metrics can be better defined and would consider the full the inter relationship between drive conditions and loss [29].

Multilayer Cofired Actuators

Traditionally, multilayer actuators have been fabricated by either a stacking process or through a multilayer cofire process [30–32]. The stacking process involves a relatively simple but time-consuming method to fabricated multilayer actuators. It involves a firing, polishing, electroding, and adhesive bonding of electrodes and ceramic layers into a stack. To achieve cost effective production methods, the cofiring process that has been successful in the multilayer capacitor industry is preferred for producing piezoelectric actuators for injectors. Furthermore, the cofiring process can also produce lower thickness layers that in turn require lower drive voltage for actuators to obtain equivalent strain. The multilayer cofire process route is outlined schematically in Fig. 5. The complexity of this process requires that all stages be optimized to maximize microstructure and densification for reliable electromechanical performance. Special consideration is required in the milling and dispersion of the piezoelectric ceramic powders in order to maximize green density. A variety of binder systems are considered for multilayer actuators, including poly-vinyl-butyl and poly-acrylic-acetate, etc. Once tapes are fabricated, thick film metal pastes for the electrodes are blended, which may include binders, dispersants, and solvents. The particulate phase for the electrode pastes have to be engineered to match the densification rate of the tapes. The thick film paste is screen-printed onto the tapes. The tapes are then stacked, laminated, and cut into the individual actuators. These so-called green or unfired parts are then taken for thermal processing, including debinding and the sintering. In both debinding and sintering, inhomogeneous strain changes can occur and must be minimized to reduce residual stresses that can create flaws, such as warping, delamination, and microcracks, in the actuator components. Details of these processes have
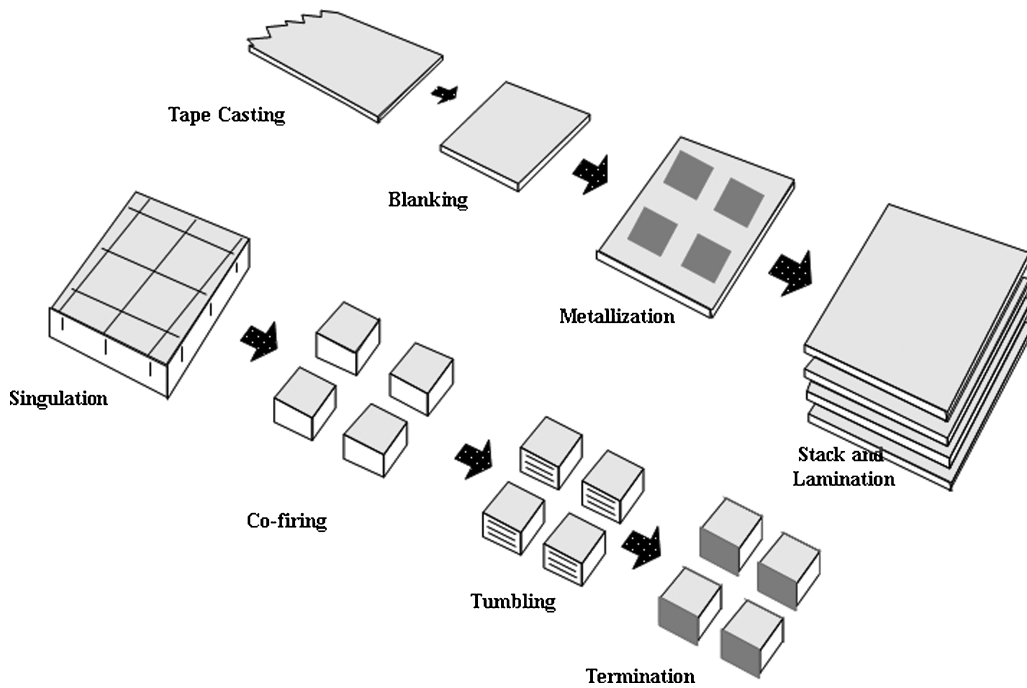
Fig. 5. Schematic outline of the basic processes required in the manufacturer of a multilayer actuators.

to be considered in relation to specific metallizations and are discussed below. The final part of the process involves "tumbling" of the components to expose the inner electrodes. This is followed by a termination process to interconnect the electrodes. The final process is the poling of the components to develop the optimum piezoelectric response within the actuator. The poling process needs to be performed in a way that maximizes the domain alignment but does not induce microcracking during the accompanying strain changes. Manufacturers often consider detailed finite element analysis of the strains induced at the electrode ceramic interfaces to limit microcracking in the poling process and optimize electrode design [33].

Metallization

The cost of metallization is of major concern for the manufacturer of piezoelectric actuators. Traditionally the cost of metallization is determined from the market price of palladium and can be up to 80% of the total material cost of the actuators basic constituents. Furthermore, the metallization selection influences a number of decisions in regard to processing and performance. Two basic strategies follow paths taken in

the multilayer capacitor market, namely a high silver alloy or a base metal. The two major metallization approaches entertained are an air-fired Ag/Pd alloy or a copper low PO_2 firing system [34]. It should be noted that Ni as a base metal alternative is not an option in Pb-based materials, as it is with $BaTiO_3$ multilayer capacitors. The reason that nickel is not compatible with PZT is that $NiTiO_3$ readily forms and thus creates reaction zones that destroy the structure and properties of the actuator [35]. In both Ag/Pd and Cu metallizations for PZT actuators, there are a number of major technical challenges. Each case is described below.

Ag/Pd Electrode Case

The Ag-Pd alloy system is a complete solid solution, as shown in Fig. 6. Pure Ag through compositions up to a 70/30 Ag/Pd alloy are typically of interest as internal electrodes for piezoelectric actuators. The composition selected will strongly influence the firing temperature of the lead-based piezoelectric ceramic, ranging from 900°C for pure Ag up to 1120°C for 70/30 Ag/Pd. For high silver, low-fire metallizations, the sintering process has to be aided with a liquid phase flux to improve

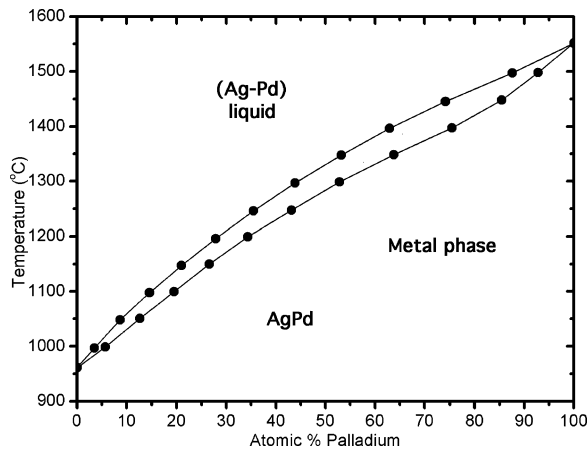Fig. 6. Complete solid solution between Ag-Pd.

(a)

(b)

Fig. 8. (a) Relative stability of PdO in different Ag-Pd alloys across the temperature range $0 \leq 90°C$, and (b) dilatometer data indicating the contraction and expansion associated with oxidation and decomposition of Ag-Pd.
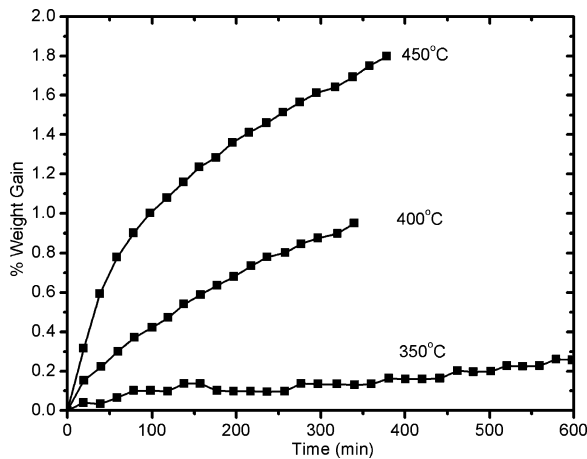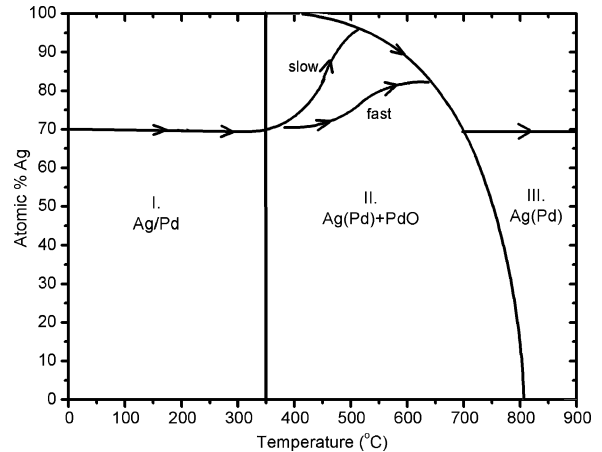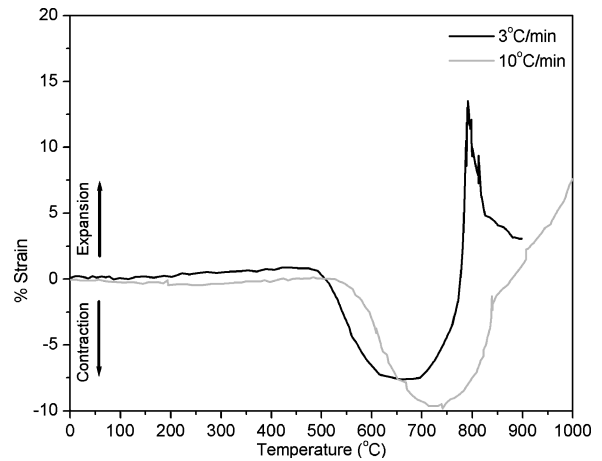

Fig. 7. Isothermal weight gain in Ag-Pd powders, at 350°C, 400°C, and 450°C.

densification. Flux selection and the basic chemical interactions will be generally discussed below.

During the binder removal process, the Ag/Pd alloyed powders can undergo a surface oxidation between 350 and 800°C, depending on Ag/Pd content [34]. Figure 7 shows % weight change due to oxidation as a function of time under isothermal conditions in a 70/30 Ag/Pd alloyed powder [34]. Figure 8(a) shows three regimes of behavior in the Ag/Pd system. Regime II shows Ag(Pd) to be stable with a PdO phase. In Regime III, the oxide phase reduces back to a metallic phase and the decomposed Pd phases re-alloys to equilibriate the homogeneous alloy. The oxidation is one source of strain created by the molar volumetric

expansion, Fig. 8(b). Also, at higher temperatures, indicated by the Regimes II and III, any entrapped PdO can release oxygen on decomposition and swell electrodes, delaminating the multilayer structure. Managing the thermal processes to minimize stress created by oxidation and reduction process of the Ag/ Pd alloy is vital during the debinding and the early sintering stages.

In addition to the oxidation and reduction processes, there are further complexities involving chemical interactions with the PbO and Bi_2O_3. At low temperatures, the oxidation of palladium Pd→PdO occurs, then in
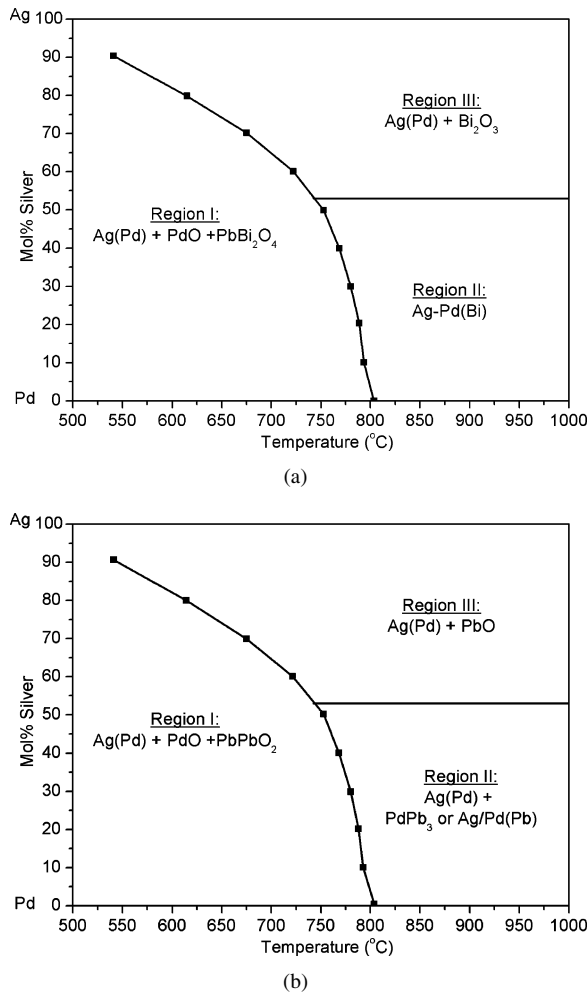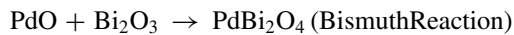
Fig. 9. Phase stability of the (a) Bismuth and (b) lead reactions with PdO in AgPd systems.

the presence of PbO or Bi_2O_3, the following lead and bismuth or lead reactions can readily occur in the temperature range from 500 to 800°C depending on the Pd content [34].

$$PdO + Bi_2O_3 \rightarrow PdBi_2O_4 \text{ (BismuthReaction)}$$

$$PdO + PbO \rightarrow PbPdO_2 \text{ (LeadReaction)}$$

The relative phase stability of these reactions are shown in Fig. 9(a) and (b). At intermediate temperatures with high palladium activity, an alloy can form. At lower activity, the $PdBi_2O_4$ (or $PbPdO_2$) decomposes to Ag(Pd) with either Bi_2O_3 or PbO. The decomposition temperatures depend on the alloy composition. On decomposition, from regime (I) to either regimes (II) or (III),

oxygen is released. The rapid release of oxygen can induce local pressure points that can induce delamination of the multilayers, requiring thermal profiles to be controlled to eliminate delamination. Holding times need to be introduced to establish the equilibrium of the AgPd alloy, as the lead or Bismuth reaction introduces a segregation. If a fast ramp rate is used, the presence of a metastable Ag(Pd(Bi)) alloy may lead to local melting of the electrodes and alter the densification rates of the Ag-Pd electrode layers, in both cases creating residual stresses that could delaminate or create voids in the actuator device [34].

With higher silver content, there is the probability of Ag_2O forming at temperatures $\sim850°C$. The Ag_2O content can then in turn diffuse and interact with the PZT piezoelectric ceramic. Interfacial reactions will incorporate Ag onto the A-site of perovskite lattice as an acceptor dopant and locally decrease the piezoelectric performance and lower the transition temperature. This interfacial layer is in series with the piezoelectric layer, giving rise to an effective decrease in performance throughout the piezoelectric actuator. It should be noted that the solubility of Ag can be ~4 mol%, but this may depend on Pb stoichiometry.

Base Metal Electrode Case

Copper electrodes can be cofired up to temperatures $\sim1000°C$, as the melting temperature is 1040°C. However, the processing window bounded by the reducing of PbO and the oxidizing of CuO complicates copper inner electrodes. If the reaction $PbO \rightarrow Pb + \frac{1}{2}O_2$ occurs, then Pb can alloy with Cu and lower the melting temperature (the atmosphere in the furnace must be controlled with N_2–H_2–H_2O and PbO (V) to maintain activities in the appropriate range). Complicating atmosphere control is local residual graphitic carbon, which can form in the oxygen deficient atmospheres during binder removal. This residual graphitic carbon can oxidize to form CO_2 and CO gases. These products can locally lower the effective $P(O_2)$ and make the atmosphere control in a furnace far more complex. Approaches to reduce the residual carbon may involve new binder systems, complex binder burnout furnace profiles, controlling temperature, $P(O_2)$, and humidity over long times, or increasing the oxidation resistance of the copper powders. In some cases, a combination of these approaches may be used. The ability to remove the binder at low temperatures and in air without the
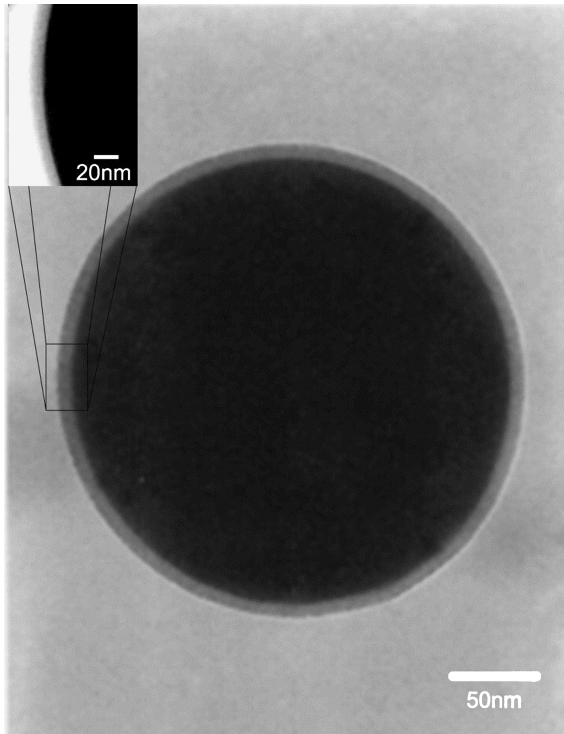
Fig. 10. TEM image of oxidation-resistant copper powders with inorganic coatings.

Fig. 11. (a) Bi-polar strain field behavior in a multilayer copper electrode actuator, and (b) multilayer copper electrode PZT actuator.

oxidation of the electrode powders is very attractive for base metal actuators. The oxidation resistance is dependent on a number of factors, including processing route such as precipitation or a chemical vapor pyrolysis. Crystallinity and surface area are both of importance in limiting oxidation, additional improvements can be obtained with either precious metal coatings or inorganic layers. Figure 10 shows a TEM image of an inorganic coated copper produced by Shoei Chemical (Japan) to passivate against oxidation.

Earlier studies by Randall et al. have successfully produced actuators, with high field strain $d_{33} \approx 390$ pC/N, using acrylate polymer binders and SiO_2-based coatings of copper powders, which allowed binder removal in air with limited copper oxidation [36]. Figure 11(a) shows the actuator bipolar strain-field dependence and (b) multilayer actuator stack with 80 μm active layers and copper inner electrodes. Even limited oxidation of copper is problematic for the same reasons discussed with Ag and Ag/Pd electrodes. The Cu^{+2} ion can act as an acceptor dopant at the interface by substitution on the B-site of the perovskite lattice. The interfacial layer again lowers the piezoelectric ac-
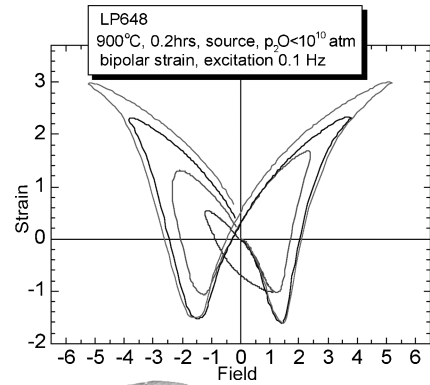
tivity across the whole device. Figure 12(a) shows a transmission electron microscopy of PZT microstructure in a copper electrode multilayer actuator. Chemical analysis with energy dispersive spectroscopy indicates Cu incorporation into lattice, Fig. 12(b).

Flux Development for Low Fire, High Piezoelectric Ceramics

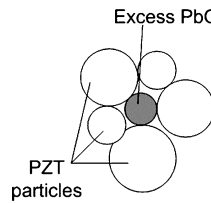Piezoelectric ceramics require careful processing in order to achieve optimized properties. In cofiring with
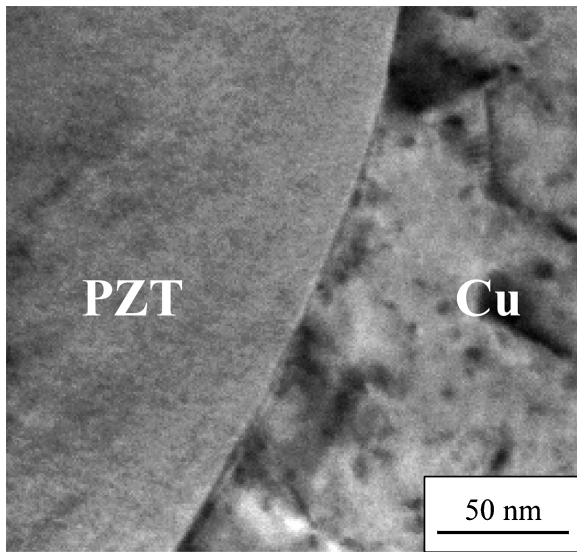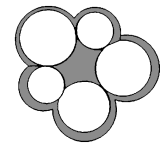
(a)
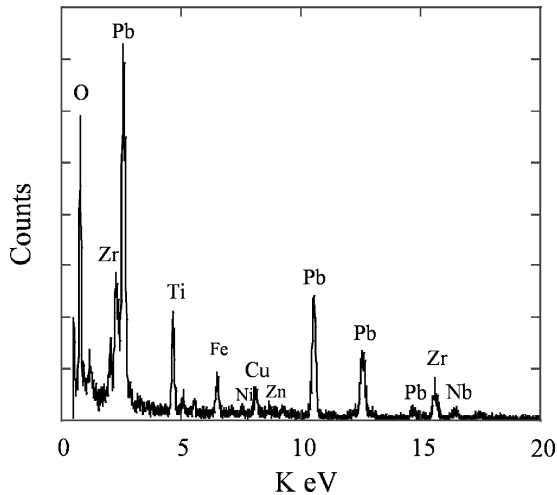
(b)

Fig. 12. (a) Interfacial microstructural imaged by conventional transmission electron microscopy in a copper multilayer actuator, and (b) energy dispersive spectroscopy indicating copper in the PZT. Spectrum taken approximately 7 μm from electrode edge. Note Ni-grids are used in the study.

Ag_{1-x}–Pd_x ($0 \leq x \leq 0.3$) or Cu, a flux is generally required. The role of a flux is to aid in the densification and grain growth to allow piezoelectric ceramics to be fired at lower temperatures without significantly affecting the piezoelectric properties. The three major phases in sintering with flux involve particle rearrangement solution reprecipitation, grain growth, and equilibriation
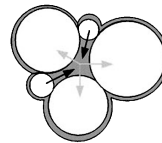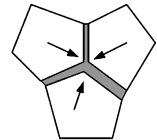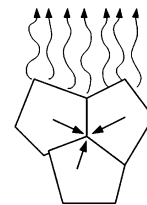
(a)
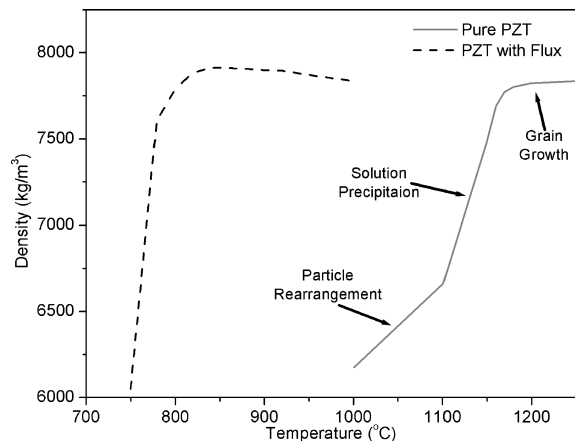
(b)

Fig. 13. (a) Schematic diagram showing mechanisms surrounding the piezoelectric ceramic sintering, and (b) comparison of sintering behavior of pure PZT and PZT with a flux added.

of the grain boundary phase [37]. Figure 13(a) shows a schematic representation (b) accompanying densification of these processes based on earlier studies [38].

There are a large number of fluxes that have been considered in the sintering of piezoelectric ceramics [39–47]. Some of these are summarized in Table 2.

Table 2. Flux chemistry for piezoelectric ceramics.

	Addition[†]	Sintering Temperature*	Melting
PbO	0.1 to 3 wt%	950 to 1000°C	886°C
LiBiO$_2$	0.1 to 1 wt%	780°C to 850°C	700°C
4PbO–B$_2$O$_3$	0.1 to 0.5 wt%	1150°C	500°C
5CdO–2SiO$_2$	0.5 to 1.0 wt%	1150°C	1100°C
Pb$_5$Ge$_3$O$_{11}$	0.2 to 1.0 wt%	950°C to 1000°C	750°C
LiF	0.5 to 2 wt%	950°C to 1050°C	875°C
CuO–PbO	1.0 wt%	950°C to 1000°C	812°C
V$_2$O$_5$	0.5 to 1.0 wt%	900°C to 1070°C	675°C
3Bi$_2$O$_3$–B$_2$O$_3$	0.5 to 1.0 wt%	1000°C to 1070°C	542°C
P$_2$O$_5$	1 wt%	1100°C to 1150°C	1050°C
Ba(Cu$_{1/2}$W$_{1/2}$)O$_3$-CuO	0.1 wt%	935°C	800°C

[†]Addition depends on composition, flux mixing, and particle reactivity.
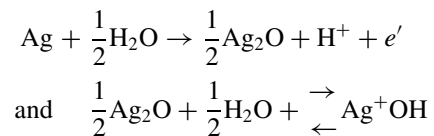*Sintering depends on flux amount, flux mixing, particle reactivity, sintering profile.

The precise wt% additions and sintering temperature depends on specific compositions and dopants making up the piezoelectric ceramic. Furthermore, the reactivity of these powders for each specific composition is also a variable, and if this is optimized at the calcination stage, less flux may be required. It should also be pointed out that the fluxes can be used in combination. When selecting a flux, the densification and grain growth is certainly part of the rationale. If the flux has some volatiles, soak time can help reduce this, but even after extrinsic annealing, excess PbO can be left in the grain boundaries at thicknesses ~1 nm and this can lower the dielectric and piezoelectric properties of the material [63]. In an earlier grain size investigation, it is noted that grain sizes <1.0 μm have a suppressed domain configuration that could limit optimal poling of domains and reduce extrinsic piezoelectric contributions. For a given well-controlled soft piezoelectric composition, maximum d_{33} levels required an average grain size of at least 2.0 μm [48, 49]. A grain boundary phase is in series connectivity with the high permittivity grains and can lower the relative permittivity and the associated piezoelectric activity [50]. It will also be shown below that intergranular grain boundary phases are fast pathways for Ag$^+$ migration under humidity and DC bias. Also, this phase can mechanically weaken the piezoelectric actuator, and fluxes should be minimized when added to the piezoelectric ceramic powder. This can be achieved by use of highly reactive piezoelectric powders and high quality milling and mixing of the flux powders. To minimize cofiring differential sintering stresses, piezoelectric powders and flux need to be mixed into the thick film pastes of the electrode materials. Once these processing features are all controlled high-level actuators can be manufactured with a variety of electromechanical characteristics and different electrode chemistries.

Electromigration and Reliability

One of the major concerns for failure in multilayer actuators driven with DC voltage or with quasi-static rectangular pulses is the electro migration of metal ions, both across a layer through grain boundaries and along the surface of an actuator [51]. This is of particular concern in high Ag-Pd alloys and pure Ag. Reliability testing in accelerated conditions of 85% relative humidity and 85°C can produce conditions of Ag oxidation followed by ionic migration and eventually reduction at the cathode, as shown in Fig. 14. These reactions are summarized below:

At the anode:

$$Ag + \frac{1}{2}H_2O \rightarrow \frac{1}{2}Ag_2O + H^+ + e'$$

$$\text{and} \quad \frac{1}{2}Ag_2O + \frac{1}{2}H_2O + \overset{\rightarrow}{\underset{\leftarrow}{}} Ag^+OH$$

The AgOH dissociates and the Ag+ is attracted to the cathode and the Ag$^+$ ion migrates under the electric potential [52]. As reduction occurs at the cathode,

$$Ag^+ + e' \rightarrow Ag$$
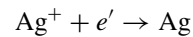
This initiates a change to the electric potential and concentrates the field, leading to dendritic electrode growth

Initial Degradation:

Cathode Rxn: $Ag^+ + e' \rightarrow Ag$ (Dendritic Growth)

Anode Rxn:

$$Ag + \tfrac{1}{2}H_2O \rightarrow \tfrac{1}{2}Ag_2O + H^+ + e'$$

$$\tfrac{1}{2}Ag_2O + \tfrac{1}{2}H_2O \Leftrightarrow Ag^+ + OH^- \Leftrightarrow AgOH$$

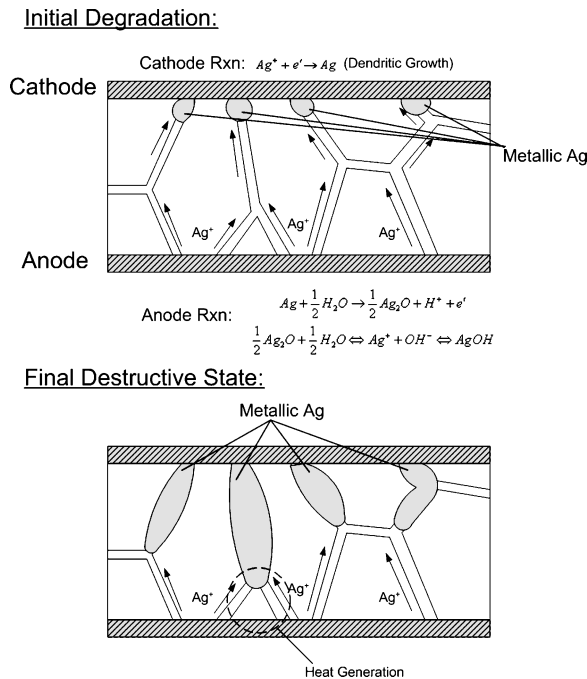Final Destructive State:

Fig. 14. Schematic of destructive effect of electro-migration of silver under DC bias.

through grain boundaries or along surfaces. Eventually failure occurs due to increased leakage current and localized heating resulting in thermal runaway.

This failure mechanism requires the application of both a d.c. bias and also H_2O humidity. Different injector designs utilize different types of driving protocols to control fuel injection, so this can be more problematic in some cases. Shorter durations of pulses will limit the degree of Ag migration and have been demonstrate in reliability to over 10^9 cycles. More detailed understanding of the specifics of the drive and cycling conditions are required to objectively access the Ag^+ electromigration issues. This includes a consideration of the degree of Ag^+ segregation as linked to the $Ag_{1-x}Pd_x$ ratio. Liu and Chen suggested a suppression of the Ag^+ ion in alloys with $x \geq 0.20$ [52]. This was suppressed by a Pd layer, but as discussed above, the degree of this segregation depends on the firing conditions and details of lead or bismuth reactions. The copper electrode systems are believed to be less problematic in this regard, but no direct evidence is available at this time in the open literature.

It should also be anticipated that the rate of Ag^+ migration depends on the composition and structure

of the grain boundaries. Earlier investigation by Kania et al. demonstrated that in closely related PMN-PT capacitors Ag^+ migration was strongly dependent on the A/B ratio in the formulations, i.e. lead-rich formulations had high Ag+ migration and lead-deficient compositions had negligible electromigration [53]. In the Pb-based piezoelectric actuators, we would expect similar trends, but we need to better understand the balance between piezoelectric performance with a given flux and the relative electromigration kinetics.

Future Directions in Multilayer Actuators

Certainly the immediate challenge for piezoelectric actuator devices lies at the manufacturing and quality control level. In terms of manufacturing, understanding the control of atmosphere in large kilns when firing many devices is essential. The control of debinding and lead atmosphere are both challenges to maintain consistent piezoelectric performance and limit delamination of the stacks. Performance needs to be correlated with all aspects of the processing, including poling conditions. Furthermore, better reliability testing is required to predict longtime performance.

In terms of new compositions, studies need to be conducted that produce high T_c and high field $d_{33} \sim 550$ pC/N in the material. Understanding of electrode interfacial behavior in both Ag-Pd and Cu metallization and processing methods is required to control the performance and reliability of multilayer actuators. There are many new opportunities for high temperature binary and ternary systems with the new Bi(Me'Me'')O$_3$ end members. Further, there are always questions and hopes for non-lead piezoelectrics. It is clear that if such a system exists, it will require a large cation on the A-site. With Cd and Pb ruled out, it appears that Bi will have to play a role in this search. Rhombohedral, Bi(Me'Me'')O$_3$ compounds have been developed, but a suitable tetragonal ferroelectric end member is missing. If ferroelectrics with no lead are required, the perovskite or other structures may have to be textured in the multilayer form to re-establish high d_{33} performance. The multilayer buildup process, in principle, could allow for this with textured seeds cast or printed in to the layers. Then during sintering, these seeds would dictate the preferred growth direction and introduce a textured alignment of the polycrystalline ceramic [54]. Figure 15 shows a schematic of this future concept.
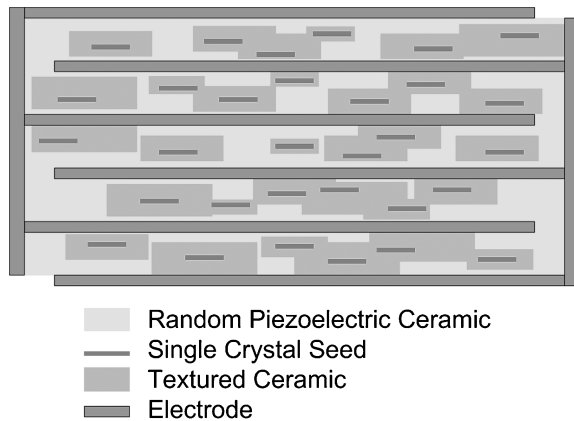
Random Piezoelectric Ceramic
Single Crystal Seed
Textured Ceramic
Electrode

Fig. 15. Templated grain growth process for production of textured piezoelectric materials.

Summary and Conclusions

This is an important time period for both the commercial realization of smart systems and the expansion of piezoelectric multilayer actuator market. It is anticipated that over the next few years, the piezoelectric market will drastically expand. This is being propelled by the automobile industry, specifically the diesel injector systems. To ensure that the cost and reliability are controlled with extensive manufacturing practice, detailed knowledge of material interactions in the piezoelectric actuator process is essential.

Most piezoelectric ceramic scientific publications only consider the basic compositions or fluxes and their relationships between microstructure and properties. These types of studies need to be broadened to address interactions with the multilayer electrode interface. In the case of AgPd electrodes, there can be segregation of Ag in the ceramic and reactions with the Pd with lead oxide or bismuth oxide. In both cases, volume changes create deleterious stresses that can cause delaminations and porosity in the multilayer actuators. In other metallizations, such as copper, there are issues in limiting lead reduction and alloying with the copper to melt electrodes from poor debinding. In addition, at high temperatures, Cu^{+2} incorporation could limit piezoelectric activity from diffusion at the interface to produce hard piezoelectric layers.

Reliabilty of the Ag-based actuators is also considered in relation to Ag migration. The exact nature of the controlling mechanisms is know, but the specifics

of the testing with accelerated lifetime testing is difficult to generalize, as it depends on drive conditions of the system.

In addition to the consideration of present day issues, we consider future trends involving high temperature piezoelectric actuators, low-lead and non-lead ceramics, and possible crystallographic texturing within the layers.

References

1. F. Zhao, M.C. Lai, and D.L. Harrington, *Prog. in Energy and Combustion Science*, **25**(5), 437 (1999).
2. P.J. Tennison and R. Rertz, *J.* of Engineering for Gas Turbines and Power, *Transactions of the ASME Engine*, **123**(1), 167 (2001).
3. *Professional Engineering*, **16**(1), 54 (2003).
4. V. Bottom, *Introduction to Quartz Crystal Unit Design* (Van Nostrand Reinhold Co., NY, 1982).
5. *IEEE Standard on Piezoelectricity* (American National Standards Institute, Washington, DC, 1976).
6. B. Jaffe, W.R. Cook, and H. Jaffe, *Piezoelectric Ceramics* (Academic Press, New York, 1971).
7. J.M. Herbert, *Ferroelectrics Transducers and Sensors* (Gordon Breach Science Publishers, New York, 1982).
8. K. Yanagiwawa, H. Kanai, and Y. Yamashita, *Jap. J. Appl. Phys.*, **34**, 536 (1995).
9. H. Ochi, *J. Am. Ceram. Soc.*, **48**, 630 (1965).
10. R.E. Eitel, C.A. Randall, T.R. Shrout, P.W. Rehrig, W. Hackenberger, and S.E. Park, *Jap. J. Appl. Phys.*, **40**(1), 599 (2001).
11. R.E. Eitel, C.A. Randall, and T.R. Shrout, *Jap. J. Appl. Phys.*, **41**(49), 2099 (2002).
12. S.J. Zhang, C.A. Randall, and T.R. Shrout, *Appl. Phys. Lett.*, **83**, 3150 (2003).
13. T. Song, R.E. Eitel, T.R. Shrout, and W. Hackenberger, *Jap. J. Appl. Phys.*, **42**, 5101 (2003).
14. C.A. Randall, R.E. Eitel, T.R. Shrout, and I.M. Reaney, *J. Appl. Phys.*, **93**(11), 9271 (2003).
15. C.A. Randall, R. Eitel, B. Jones, T.R. Shrout, D.I. Woodward, and I.M. Reaney, *J. Appl. Phys.*, **95**(17), 3633 (2004).
16. C.A. Randall, R.E. Eitel, C. Stringer, T.H. Song, S.J. Zhang, and T.R. Shrout, *Piezoelectric Single Crystals and Their Applications*, edited by S. Trolier-McKinstry, L.E. Cross, and Y. Yamashita (Published Privately, University Park, PA, 2004) pp. 346–365.
17. H. Thomann, *Zeitschrift für Angewandte Physik*, **20**, 554 (1966).
18. F. Kulscar, *J. Am. Ceram. Soc.*, **42**(7), 343 (1959).
19. I. Ueda, *Jap. J. Appl. Phys.*, **11**(4), 450 (1972).
20. G.H. Haertling, *J. Am. Ceram. Soc.*, **50**, 329 (1967).
21. K. Carl and K.H. Hardtl, *Phys. Sol. Stat.* (A), **8**, 87 (1971).
22. L. Eyrand, P. Eyrand, and B. Claudel, *J. Sol. Stat. Chem.*, **53**, 266 (1984).
23. P. Gerthsen, K.H. Hardtl, and N.A. Schmidt, *J. Appl. Phys.*, **51**(2), 1131 (1980).
24. G. Arlt, H. Dederichs, and R. Herbert, *Ferroelectrics*, **74**, 37 (1987).

25. L. Rayleigh, *Philosophical Mag.*, **23**(142), 225 (1987).
26. D.V. Taylor and D. Damjanovic, *J. Appl. Phys.*, **82**(4), 1973 (1997).
27. D. Damjanovic and M. Demartin, *J. Phys. Condensed Matter*, **9**, 4943 (1997).
28. D.A. Hall, *J. Mat. Science*, **36**, 4575 (2001).
29. D. Damjanovic and G. Robert, *Piezoelectric Materials in Devices*, edited by N. Setter, (Switzerland), pp. 353–388.
30. L.J. Bowen, T.R. Shrout, W.A. Schulze, and J.V. Biggers, *Ferroelectrics*, **27**, 59 (1980).
31. S. Takahashi, A. Ochi, M. Yonezawa, T. Yano, T. Hamatsuki, and I. Fukui, *Ferroelectrics*, **50**, 181 (1983).
32. K. Uchino, *Acta Mater.*, **46**(1), 3745 (1998).
33. K. Lubitz, C. Schuh, T. Steinkopff, and A. Wolff, *Piezoelectric Materials in Devices*, edited by N. Setter (Switzerland), pp. 183–194.
34. S.F. Wang, J.P. Dougherty, W. Huebner, and J.G. Pepin, *J. Am. Ceram. Soc.*, **77**(12), 3051 (1994).
35. P. Groen, *American Ceramic Society Meeting* (American Ceramic Society, Cocoa Beach, 1993).
36. C.A. Randall, A. Kelnberger, T. Shrout (in progress).
37. Y.M. Chiang, D. Birnie III and W.D. Kingery, *Physical Ceramics* (J. Wiley & Sons, Inc., New York, Cincinnati, Toronto, Brisbane, Singapore, 1996).
38. M. Kondo and K. Kurihara, *J. Am. Ceram. Soc.*, **84**(11), 2469 (2001).
39. R.B. Atkin, R.L. Homan, and R.M. Fulrath, *J. Am. Ceram. Soc.*, **54**, 113 (1971).
40. A.I. Kingon and J.B. Clark, *J. Am. Ceram. Soc.*, **66**(4), 256 (1983).
41. K. Murakami, D. Mabuchi, T. Kurita, Y. Niwa, and S. Kaneko, *Jap. J. Phys.*, **35**, 5188 (1996).
42. X.X. Wang, K. Murakami, O. Sugiyama, and S. Kaneko, *J. European Ceram. Soc.*, **21**, 1367 (2001).
43. D.E. Wittmer and R.C. Buchanan, *J. Am. Ceram. Soc.*, **64**, 485 (1981).
44. X. Wang, P. Lu, and W. Xue, in *Proceedings of Sixth International Symposium on Applications of Ferroelectrics* (ISAF, 1992) USA, pp. 585–587.
45. C.H. Wang and L. Wu, *Jap. J. Appl. Phys.*, **32**(7), 3204 (1993).
46. T. Hayashi, T. Inoue, and Y. Akiyama, *J. European Ceram. Soc.*, **29**, 999 (1999).
47. A.K. Saha, D. Kumar, O. Parkash, A. Sen, and H.S. Maiti, *Mat. Res. Bull.*, **38**, 1165 (2003).
48. C.A. Randall, N. Kim, J.P. Kucera, W.W. Cao, and T.R. Shrout, *J. Mat. Res.*, **8**(4), 880 (1993).
49. G. Helke, S. Seifert, and S.-J. Cho, *J. European Ceramic Soc.*, **19**, 1265 (1999).
50. C.A. Randall, A.D. Hilton, D.J. Barber, and T.R. Shrout, *J. Mat. Res.*, **8**(4), 880 (1993).
51. K. Nagata and J. Thougrueng, *Jap. J. Appl. Phys.*, **37**(9B), 5306 (1998).
52. J.C. Liu and J.Y. Chan, *Mat. Chem. and Physics*, **43**, 256 (1996).
53. H. Kanai, O. Furukawa, S. Nakamura, and Y. Yamashita, *J. Am. Ceramics Soc.*, **76**(2), 454 (1993).
54. T. Takeuchi, T. Tani, and Y. Saito, *Jap. J. Appl. Phys. Part 1*, **9B**, 5553 (1999).
55. T. Tani, *J. Kor. Phys. Soc.*, **32**, S1217 (1998).